

AEROSOL RETRIEVAL AND ATMOSPHERIC CORRECTION

E. VERMOTE, NAZMI EL SALEOUS AND B. N. HOLBEN

NASA / Goddard Space Flight Center,

Greenbelt, MD, 20771,

U.S.A.

ABSTRACT. Remote monitoring of global-scale parameters and their change requires the correction of atmospheric effects. Apart from clouds, water vapour and aerosols constitute the primary limitations for the remote sensing of surface features in the AVHRR visible and near-infrared channels. The following chapter presents methods for correcting data in these channels for water vapour and aerosol interference using AVHRR data alone. Included are two methods for aerosol retrieval which are applicable for AVHRR visible and near-infrared radiance data. The first method is the “*dark target*” approach that currently has applicability over oceans and dense dark vegetation. The method has been shown to have an accuracy of approximately 0.1 for optical thickness estimations. The second method, the “*contrast reduction*” method, has a similar accuracy and is complimentary to the first method in that it can be applied in regions of invariant surface cover, such as those where little or no green vegetation grows.

The dark target retrieval is demonstrated on a global-type data set over oceans and land targets. Included is a discussion of calibration, water vapour correction and cloud-screening methods. A method of atmospheric correction for the Pinatubo stratospheric aerosol is then given and applied to part of the same global data set. As validation of the method, data from years after the Pinatubo eruption are seen to compare well with data from years before the eruption, once the Pinatubo stratospheric aerosol correction has been applied.

1. Aerosol Retrieval: A review of two different approaches

Aerosols have two opposite effects on visible and near-infrared satellite signals. First, they increase the signal measured at the sensor by adding a contribution called the “intrinsic atmospheric reflectance” (caused by photons that are reflected to the atmosphere before interacting with the target). Second, they decrease the amount of light reaching the target, the so-called “transmission effect” (caused by absorption and scattering of photons en route to the target or sensor).

There are basically two methods of determining and isolating the effects of aerosols from the visible and near-infrared satellite signals. In the first method, retrieval of aerosol amount may be achieved from visible (red wavelength) observations of dark targets such as still water bodies or dark dense vegetation, hence its name “*dark target approach*”. In the second method, the variation in the amount of transmission may be estimated by considering an invariant target which will allow a relative correction to be applied. This latter approach is called “*contrast reduction*”.

Both approaches have been successfully applied to data from the Landsat TM sensor and have shown good potential for determining the optical thickness with an accuracy of

up to 0.1 in the red portion of the electromagnetic spectrum (specifically at 0.55 μm). The application of these methods to global data sets implies the establishment of: (1) an operational criterium to identify dark targets, and (2) operational criteria to identify and check the spatial homogeneity and invariance of reference targets.

In this chapter we present the first application of both atmospheric correction methods to global-scale full-resolution and GAC AVHRR data, and further define the criteria required for their global operational application (as well as an estimate of their accuracy).

2. Conceptualization of aerosol retrievals

The methods for atmospheric retrievals are based on the determination of the concentration of atmospheric aerosol (or the aerosol optical thickness, τ_a) from radiances taken from the image itself. The atmospheric effect on the image may be described by:

$$L(\tau_a) = L_o(\tau_a) + F_d(\tau_a)T(\tau_a)\rho/(1-s(\tau_a)\rho), \quad (1)$$

and it is composed of two parts: the atmospheric path radiance L_o due to photons scattered by the atmosphere to the sensor without being reflected by the surface, and the atmospheric effect on the transmission of the downward flux, F_d , and the upward transmission, T . $s(\tau_a)$ describes the multiple interaction between the ground and atmosphere. Both atmospheric effects have been used in the past to determine the aerosol optical thickness, and their derivation from AVHRR data is described in the following sections.

2.1. DETERMINATION OF AEROSOL OPTICAL THICKNESS USING PATH RADIANCE

2.1.1. *General.* In order to determine the aerosol optical thickness from the path radiance, the second term in Equation 1 must be small, so that the uncertainty in the surface reflectance, ρ , will have a minimal effect on the determination of τ_a . A variety of forests, forming dense, dark green canopies have low reflectance, only 1-2% in the red channel, *e.g.* deciduous forest (Kaufman and Sendra 1988), coniferous forest (Deering and Eck 1991, Kriebel 1977), hardwood and pine forests (Kimes *et al.* 1986, Kleman 1987) and tropical forests (Kaufman *et al.* 1992). Therefore, large patches of forests in generally urban or rural areas can be used to derive the aerosol optical thickness and subsequently to apply atmospheric correction. This method we term DDV (dense dark vegetation) and it appears appropriate for the coarse resolution AVHRR data in areas where there are large expanses of dense dark targets such as vegetation (*i.e.* forest) or water.

The accuracy of the determination of the aerosol optical thickness using this path radiance method depends on the accuracy of the assumed reflectance of the dark objects (*e.g.* vegetation or water) and on the ability of estimating the aerosol scattering phase

function and single scattering albedo. The total error inherent in this method (including the effect of uncertainty in the surface reflectance and assuming a good calibration) was estimated as $\Delta\tau_a = \pm 0.10$ (Kaufman and Sendra 1988) for Landsat MSS data. In the process of correcting the image for the atmospheric effects, the errors due to uncertainty in the aerosol phase function partially cancel out (Kaufman and Sendra 1988) since the same phase function that is used to derive the aerosol optical thickness is also used in the correction process. As a result, the error in the derived surface reflectance is mainly affected by the accuracy of the assumed reflectance of the dark surface ($\Delta\rho = \pm 0.01$). Extrapolation of the optical thickness to other channels (from the red to the near-infrared) can be done, but with an uncertainty of $\Delta\tau_a = \pm 0.05$, and for the path radiance an uncertainty of $\Delta L = \pm 0.002 \cdot F_0 / \pi$ (Kaufman 1991).

An aerosol retrieval scheme is possible with one of two methods provided that surfaces with known characteristics can be identified. The required characteristics are: very low surface reflectance for the path radiance method, and a number of invariant contrasting targets for the contrast reduction method. The following sections review ways of delineating such suitable areas.

2.1.2. Dense dark vegetation. This method can be applied to images for which there is *a priori* knowledge that dense vegetation is present, taking into account the geographic location and season in which the image was taken (for geographic distribution see Figure 12 of Kaufman and Sendra (1988)). Some minimal fraction of pixels covered by the dense vegetation has to be assumed (the actual fraction may be larger). It is further assumed that the spatial distribution of these pixels is dense enough to cover any spatial variability in the aerosol concentration. Two approaches are possible to determine, on a statistical basis, which pixels are covered by dense dark vegetation.

Determination based on vegetation index examination. This method is described in detail by Kaufman and Sendra (1988) in which they used Landsat MSS data. The following is a brief summary of the method modified for the AVHRR Channel 1. The vegetation index, NDVI, can be used to determine pixels that have the densest, greenest and darkest vegetation in the image. The absolute value of the NDVI depends, amongst other things, on the atmospheric effect (Holben 1986, Tanré *et al.* 1992), viewing and illumination geometry (Holben and Fraser 1984) and surface bidirectional reflectance (Deering and Eck 1991, Kimes *et al.* 1986, Lee and Kaufman 1986, Tanré *et al.* 1992). As long as the image to be analysed is small (*e.g.* less than 200 km by 200 km) aerosol concentration, and the resulting atmospheric effect is more likely to be uniform, geometrical effects will be minimised and pixels that correspond to the densest vegetation should have the highest NDVI values. A small size image is also more likely to yield uniformity in water vapour concentrations. Pixels that correspond to dense, dark vegetation (DDV) are then separated from other vegetated pixels, *i.e.* those having the lowest reflectance in the near-infrared channel. These pixels are also expected to have low, well-defined reflectance values in the visible channel that can be used to determine the aerosol optical thickness. However, large variations in aerosol concentrations from one part of the image to another may also cause large variations in NDVI values across the image, and may therefore lead

to the erroneous identification of dense dark vegetation areas. Consequently, this method should not be used in regions with highly variable aerosol concentrations (Kaufman and Sendra 1988).

Determination based on radiance at 3.75 μm . Radiance at 3.75 μm , the wavelength at which the AVHRR channel 3 is sensitive, is affected both by thermal emission and by reflection of the weak solar irradiance at this wavelength. Depending on the value of the surface reflectance and temperature, either of these two effects can dominate. The complex characteristics of this channel make it hard to use, but some widely different applications do emerge. For example, this channel on the AVHRR has been used to determine the size/phase of cloud drops (Arking and Childs 1985), has been shown to be very sensitive to variation in the surface temperature (Kerber and Schutt 1986), and is the most sensitive channel to detect the difference between mature forest and vegetated but deforested areas (Malingreau and Tucker 1988, Tucker *et al.* 1984, and Malingreau *et al.* later in this book).

This latter quality suggests application to aerosol retrieval using the DDV. In an image of mixed surface cover, forest is expected to have the lowest radiance in this channel (except for water, clouds and snow). Due to evaporation, forest is usually cooler than regions with lower density vegetation or bare soil. Also, vegetation has low reflection in this channel due to the absorption of liquid water in live vegetation, and forest decreases this reflection even further by trapping incoming sunlight due to the multilayer canopy structure. These characteristics, as depicted in the radiance of the 3.75 μm channel, in contrast to the visible channel and NDVI depictions, are illustrated in a transect taken from a remarkably cloud-free AVHRR scene over the Amazon forest (Figure 1). It can be seen that variations in the reflectivity of the red channel, caused by variation in the surface cover, are highly correlated with the vegetation index, and are even more apparent in the value of the 3.75 μm channel which has a smaller scan angle effect.

Since most aerosol types have a small particle size, and high transmissivity index in the 3.75 μm wavelength range (Holben *et al.* 1990, Kaufman *et al.* 1992, Shettle and Fenn 1979, Whitby 1978) the aerosol layer is mostly transparent in this channel. Therefore, the selection of dense vegetation pixels is expected to be nearly independent of the aerosol loading and the 3.75 μm channel should be better than the NDVI in selecting the dense dark vegetation pixels. However, it is important to bear in mind that desert dust may behave differently in this respect due to its larger particle size.

2.2. DETERMINATION BASED ON ATMOSPHERIC TRANSMISSION

Determination of the aerosol optical thickness from the atmospheric transmission (second term in Equation 1) is based on the ratio of the transmission among several images and is termed contrast reduction. Tanré *et al.* (1988) suggested and applied this method to several Landsat TM images taken over an arid region. The variation in the transmission is determined from the variation of the difference between the radiance from pixels located a specified distance apart. From Equation 1, the difference of apparent radiance ΔL^*_{ij} between two adjacent pixels (i,j) and ($i,j+1$), where i and j are the geographical

coordinates expressed in line and column numbers, may be related to the actual ground reflectance difference $\Delta\rho_{ij}$ by

$$\Delta L_{ij}^*(\tau) \cong \Delta\rho_{ij} \frac{T(\tau_a, \mu_v) F_d(\tau_a, \mu_s)}{1 - \langle \rho \rangle s \cdot 2} \quad (2)$$

where $\langle \rho \rangle$ is the mean reflectance of the two pixels.

If the method is applied to a group of images which includes a relatively clear image (for which the optical thickness is available or estimable), the actual $\Delta\rho_{ij}$ can be derived and the optical thickness for each of the images can then be estimated from Equation 2 (Tanré *et al.* 1988). The derived optical thickness is independent of the aerosol scattering phase function, but depends on the single scattering albedo, ω_0 , and the asymmetry parameter of the aerosol.

BRAZIL, JULY 23, 1990.

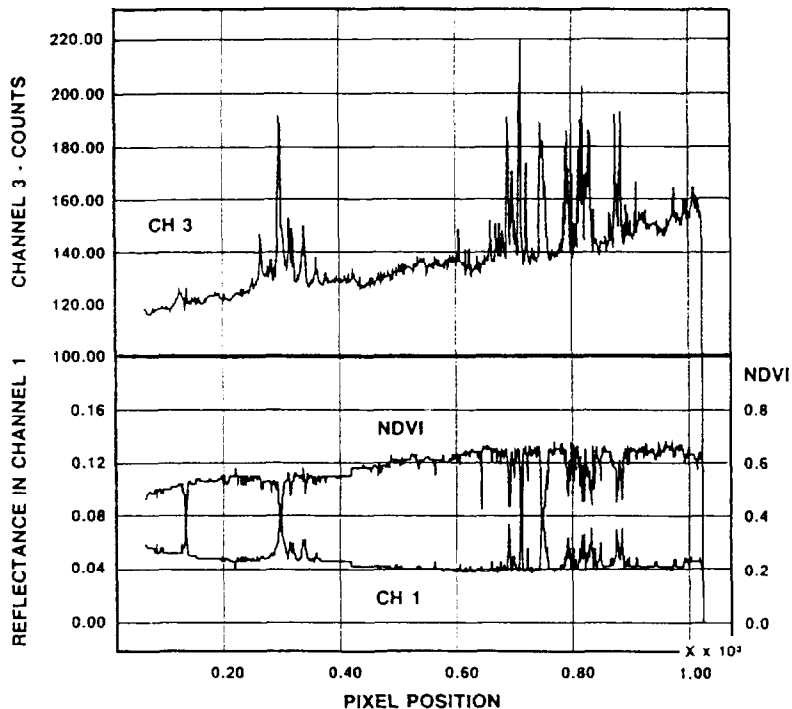


Figure 1. AVHRR bands 1 and 3 are plotted versus scan angle for a transect across the southern Amazon forest dominated by Dense Dark Vegetation. Note the increased sensitivity in band 3 relative to the NDVI for surface variations.

The reduction in contrast for Landsat TM and AVHRR resolution as a function of the aerosol optical thickness, for $\theta_s = 60^\circ$, a nadir observation and a continental aerosol model was simulated (and is shown in Figure 2). The contrast reduction is 40% lower for the AVHRR but still large enough for hazy or dusty conditions in order to be applied in arid or semi-arid regions where large and variable aerosol concentrations prevail (Holben *et al.* 1991).

To express the contrasted character of the target, $(\Delta\rho_{ij})$, we use the structure function concept, noted $F_s(d)$, and defined by:

$$F^*s(d)^2 = \frac{1}{n^*(m-d)} \sum_{i=1}^n \sum_{j=1}^{m-d} (\rho_{ij} - \rho_{i,j+d})^2 \quad (3)$$

where d is the distance between the pixels and $n^*(m-d)$ is the total number of pixels within the target for the structure function $F_s(d)$. From Equations (2) and (3), the structure function observed from the satellite $F^*s(d)$ and the actual structure of the surface $F_s(d)$ are related by :

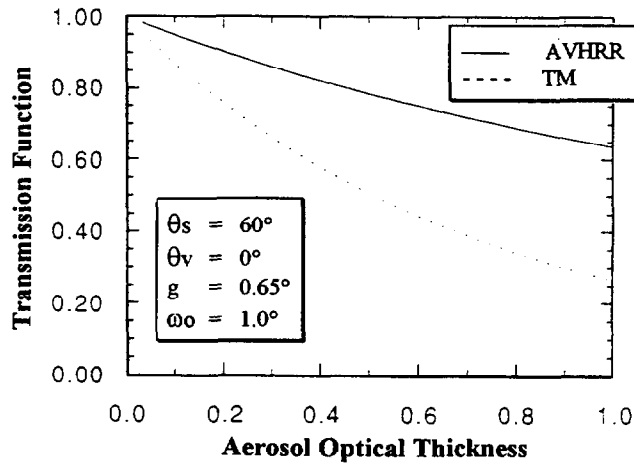


Figure 2. The transmission function response for AVHRR band 1 and TM 3 are simulated for a large range of aerosol optical thicknesses. The sensitivity of the AVHRR band (although not as great as the TM) is adequate for retrieval using the transmission function method.

$$F^*s(d) = F_s(d) \frac{T(\tau, \mu_v) F_d(\tau, \mu_s)}{1 - A^*s} \quad (4)$$

where A is the mean albedo of the target .

Provided that $F_s(d)$ is known and invariant, the satellite measurements allow us to estimate the aerosol optical thicknesses by means of the transmissions functions of Equation 4.

3. Demonstration of aerosol optical thickness retrieval methods

The two methods described above (DDV and Contrast Reduction) generally apply to different cover types. Obviously, the DDV approach is most appropriate in areas where dense dark vegetation is evenly distributed across a scene, in patches of at least more than one pixel size. The contrast reduction method applies more easily to areas devoid of any vegetation as long as there are large contrasts in the surface reflectance in single scenes, which remain invariant between scenes. Therefore, we have chosen two sites to illustrate the two techniques: the Amazon basin for the DDV approach and the Sahel in Mali for the contrast reduction approach. Some ground information was available at both sites.

3.1. THE DENSE DARK VEGETATION METHOD

This method was applied to four 1989 AVHRR 2 x 2 degree scenes with a pixel resolution of 1 km over the Amazon basin in Brazil. The aerosol optical thickness was measured by the authors on days 247 and 249. Two Amazon Basin sites which both contain large tracts of dense forest canopies were chosen, Alta Floresta and Santarem. In the area of our ground observations, significant deforestation by burning had resulted in large areas of non-forest canopies and bare ground. A third site of intensive forest burning was chosen over the state of Rondonia to illustrate differences in the methods under conditions of spatially variable concentrations of aerosols. Both DDV methods previously described (determination by VI examination, and by examination of radiance at 3.75 μm) were applied to delineate the most suitable areas of dense dark vegetation. Ground observations were made from a five-band sun photometer taken at a single location within the scenes analysed, and were used to verify the AVHRR retrieved aerosol optical thicknesses.

The retrieved aerosol optical thickness in Channel 1 was computed for the NDVI and 3.75 μm techniques according to the method described in the previous section. Cloud screening was applied to images from all dates using a simple interactive thermal 11.0 μm threshold and a primitive cloud shadow approximation based on an assumed cloud height and illumination direction. This eliminated about 20 to 80% of all pixels from the various scenes due to the afternoon broken cumulus cloud layer.

The optical thicknesses measured for each site and the mean values retrieved by each method (days 247 and 249) generally agree to within 0.2. For the uniformly distributed optical thickness (standard deviation in the 3.75 μm method is < 0.05), the NDVI and 3.75 μm methods agree within $\Delta\tau_a = 0.03$. For a day when the optical thickness was very non-uniform and smoke plumes were also observed (252, 1987- $\sigma_{3.75} = 0.27$), $\tau_{a3.75}$ is larger than $\tau_{a\text{NDVI}}$ by 0.24 (Table 1). For day 247 the mean value of the NDVI method is within 0.01 of the ground observation and the 3.75 μm method exceeds the ground observation by 0.11. The standard deviation for the 3.75 μm method, however, is large (Table 1). This is illustrated by plotting the difference of the mean retrieved aerosol optical thickness by the two methods against the standard deviation from the 3.75 μm method (Figure 3). A clear trend of increasing inhomogeneity (larger $\sigma_{3.75}$) results in a larger disparity between the methods. A frequency histogram of day 249 at Alta Floresta indicates that the 3.75 μm method retrieves a much broader range of aerosol optical thicknesses than does the NDVI on this date, suggesting a lack of uniformity in the aerosol optical thickness across the scene, and a violation of the basic assumption of the NDVI method (Figure 4a). In contrast, the frequency histograms for day 259 are nearly identical and the range in retrieved aerosol is small (Figure 4b). In this case, the techniques appear equivalent.

The sensitivity of the two methods to aerosol non-uniformity is further illustrated by plotting the brightness temperature at 3.75 μm and the NDVI for the selected DDV pixels in each method against the retrieved aerosol optical thickness for day 249 (Figures 5 and 6). By relaxing the thresholds for the NDVI technique, the range of the retrieved optical thicknesses was matched to the range in retrieved values using the 3.75 μm technique. While the NDVI decreases as a function of τ_a , (Figure 6) the $T_{3.75}$ is independent of τ_a (Figure 5) which shows the advantage of the 3.75 μm technique for non-uniform aerosol layers. The results clearly demonstrate the importance of the assumption of a uniformly distributed aerosol optical thickness over the scene in question, in order to successfully retrieve the aerosol optical thickness by the NDVI method.

Table 1. Comparison between aerosol optical thickness derived from each of the methods and ground measurements.

Day/Year	Geometry ($^{\circ}$) $\theta_s/\theta_v/\phi_v$	Aerosol Optical Thicknesses (τ_a)				Location/ comments
		NDVI Method	3.75 μm method	Ground obs.	Cloud fraction	
247/89	40.9/-43.4/139	0.39 \pm 0.02	0.51 \pm 0.08	0.40	0.70	Alta Floresta
249/89	35.9/-17.1/137	0.40 \pm 0.02	0.58 \pm 0.13	0.52	0.26	Alta Floresta
249/89	35.0/-34.2/148	0.36 \pm 0.04	0.33 \pm 0.02	0.16	0.67	Santarem
250/89	33.6/-1.0/111	0.51 \pm 0.02	0.58 \pm 0.11	ND	0.68	Alta Floresta
259/89	34.2/-9.4/143	0.33 \pm 0.02	0.36 \pm 0.05	ND	0.79	Alta Floresta

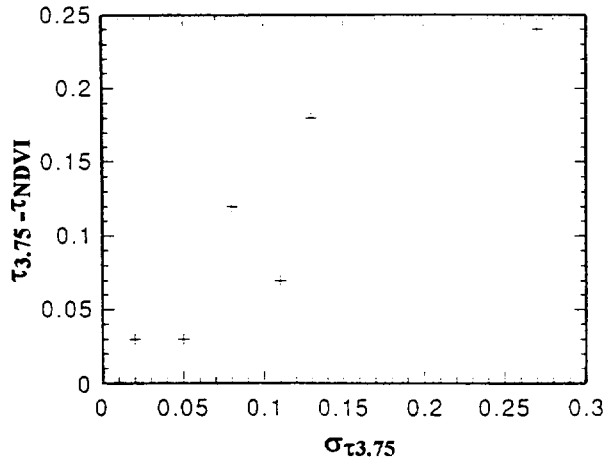
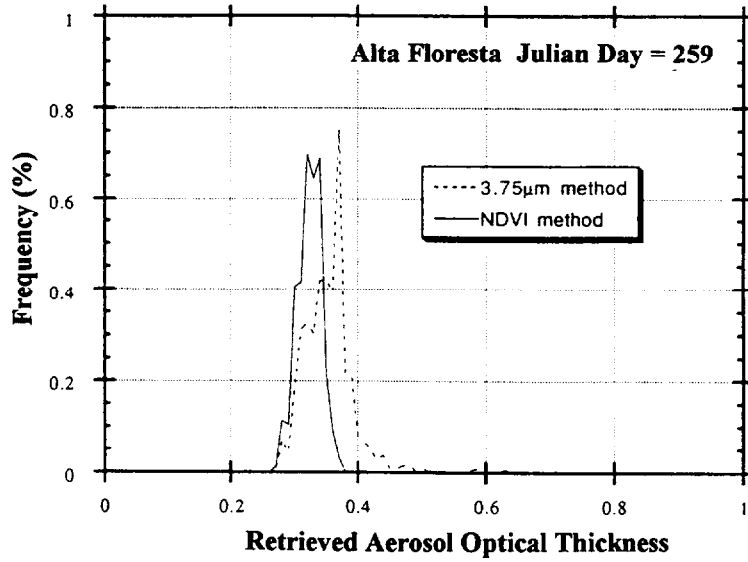
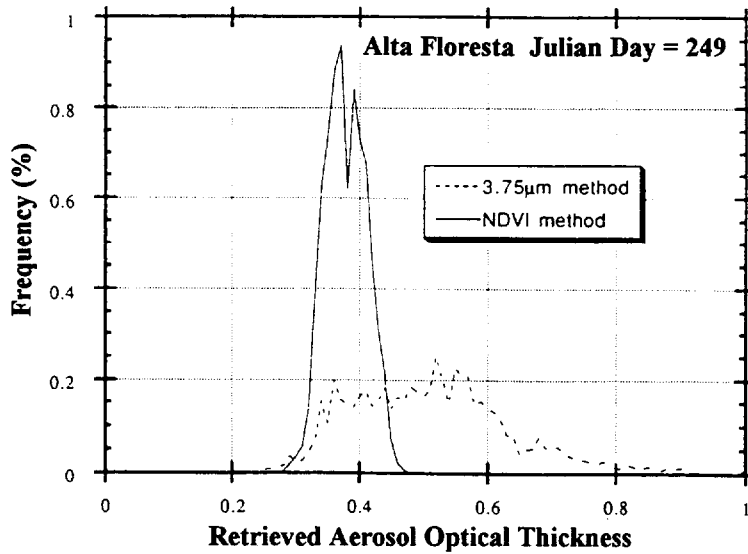


Figure 3. The τ_a difference between the 3.75 μm and NDVI methods is plotted against the standard deviation ($\sigma_{\tau_{3.75}}$) of the aerosol optical thickness for scenes analysed. As the aerosol inhomogeneity increases (high $\sigma_{\tau_{3.75}}$) the difference between the two methods increases illustrating the utility of the 3.75 μm method under these conditions.

The last site considered is in Santarem, Brazil. Ground observations made at the airport approximately 1.5 hours after the AVHRR overpass showed an aerosol optical thickness of 0.16 for AVHRR Channel 1 and the visibility was observed to be greater than 15 km for the region, which had numerous small cumulus clouds present at the time. The retrieved values for both methods are similar, near 0.3, and nearly double the measured value (Table 1). Several factors may be responsible for the disparity between the retrieved and measured values: (i) the measured value at the airport is simply one observation that may not be representative of the retrieval area; (ii) the AVHRR viewed in the hot spot direction for the Santarem scene and this would cause an overestimation of the retrieved aerosol amount (although the *magnitude* of the effect is not known); (iii) because the area surrounding Santarem is populated, we may well expect cultural activities to increase the surface reflectance by slightly more than our assumed 0.02, which would also increase our value of the retrieved aerosol optical thickness; and (iv) the Santarem image (as with many AVHRR afternoon images in this area) is contaminated with cumulus cloud formations which increases the likelihood of incorporating subpixel clouds in the assumed "cloud free" radiances used for the retrievals, and this could also lead to overestimation of the retrieved aerosol optical thickness. With regard to the final factor, it is nonetheless encouraging to retrieve reasonable (though probably high) τ_a values even between the clouds. Recognizing the effect of sub-pixel clouds on the retrieved values, we are investigating further methods of minimising it.



(a)



(b)

Figure 4. Frequency histograms of NDVI and channel 3 methods for aerosol retrieval on a hazy day (a) and clear day (b) in Alta Floresta, Brazil.

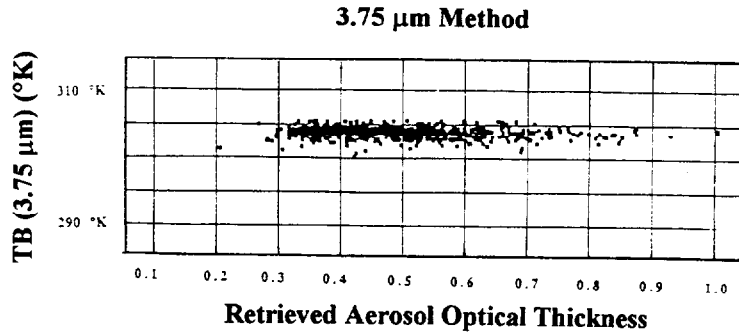


Figure 5. The sensitivity of the 3.75 μm methods to aerosol heterogeneous distributions. For optical thicknesses from 0.25 to 1.0 the 3.75 μm method varies by only 4 degrees K.

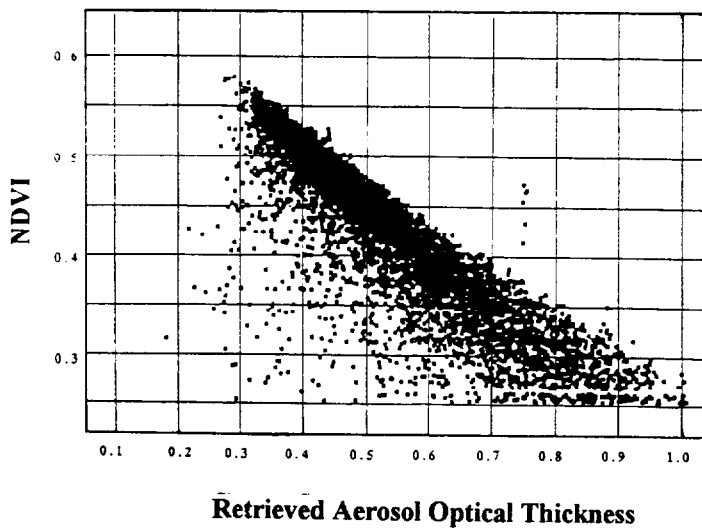


Figure 6. The sensitivity of the NDVI methods to aerosol heterogeneous distributions is illustrated. For optical thicknesses from 0.25 to 1.0 the NDVI varies by a factor of two.

Considering our lack of knowledge of the true surface reflectance in Channel 1 for various conditions and our current uncertainty in setting thresholds *a priori* for both methods, we used the 5S code (Tanré *et al.* 1990) to estimate the uncertainty in retrieved aerosol optical thickness for a 0.01 departure from the assumed 0.02 surface reflectance. The difference is approximately 0.15 and considering other sources of error, a deviation of 0.2 from the true value in some cases is not unreasonable.

3.2. THE CONTRAST REDUCTION METHOD

As described before, this method may be applied to images in which it is possible to find a number of contrasting targets which have a reflectance that is invariant in time. Such conditions occur typically in arid and semi-arid regions where the DDV method cannot be applied, for example in the Sahel of Mali, from where our case study example is drawn. We selected six AVHRR images for which contemporaneous ground measurements were available, one at the end of the growing season (86/10/3, day 276) and 5 within the dry season, 09/12/86 (day 343), 10/12/86 (day 344), 19/12/86 (day 353), 05/01/87 (day 005) and 15/01/87 (day 015). The selections have similar geometrical conditions but widely varying atmospheric conditions (Table 2).

Within the image, three sub-zones were selected (Figure 7). Zone 1 has two prominent features, the Niger river and a low range of the mountains in the east; Zone 2, west of the first, includes the Niger river and bright pixels to the north; Zone 3, further south, includes a small portion of the Niger river but has no other prominent features (Figure 7). Gao airport, the site of the ground observations, is common to all zones and is indicated by (+). The three zones are all regions of 50 by 50 pixels in size about 80 km square, the pixel size being 1.5 km after remapping. The data were remapped and registered with one pixel r.m.s. accuracy, to overlay the same geographical area for the different days.

Table 2. Geometric and atmospheric conditions at Gao, Mali for the six days.

Day of Year	θ_s	θ_v	ϕ_v	τ_a	U_{H_2O}
276	45.6	54.4	50	0.40	4.20
343	14.0	60.0	34	0.11	1.53
344	7.2	58.0	210	0.08	1.44
353	1.6	58.4	210	0.63	0.66
005	30.4	60.0	33	0.40	1.18
015	17.2	56.8	32	0.35	1.27

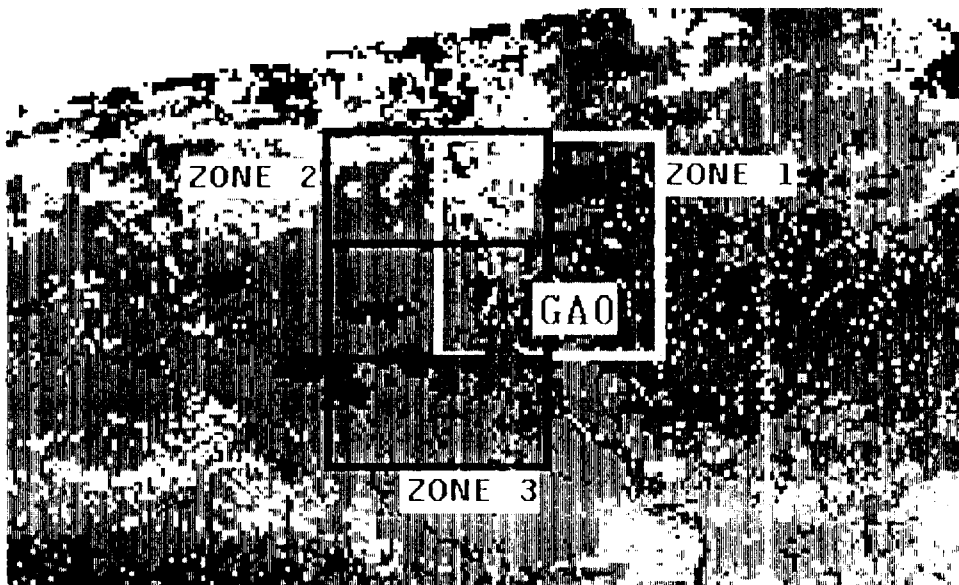


Figure 7. The NDVI computed from the reference image shows the location of the three zones each 40 LAC pixels square used for the contrast reduction method. The ground observation site at Gao, Mali, is common to all zones.

Results of the structure function (Equation 3) are plotted against distance from any given pixel within the three zones. This illustrates how the structure function changes due to the influence of variable aerosol loading on each day and the importance of selecting an area of sufficient contrast to observe the atmospheric effect. For zone 1 (Figure 8a), the magnitude of the structure functions is in good agreement with ground optical thickness measurements (Table 2). The largest structure is observed for the clearest day (344) with no difference for day 343 which has similar atmospheric conditions. Days 276, 005, and 015 all have lower magnitudes consistent with the measured intermediate aerosol optical thicknesses. Finally, the most turbid day (353) has the lowest structure function. The same conclusions apply to zone 2 except that day 276 appears as the most turbid day (Figure 8b). The magnitude of the structure is slightly smaller (10%) for all days than for zone 1 because the contrasting mountain feature is not present. For zone 3 (Figure 8c), the magnitude is only half that of zone 1, and the different days do not appear to be ordered in relation to the ground aerosol optical thickness.

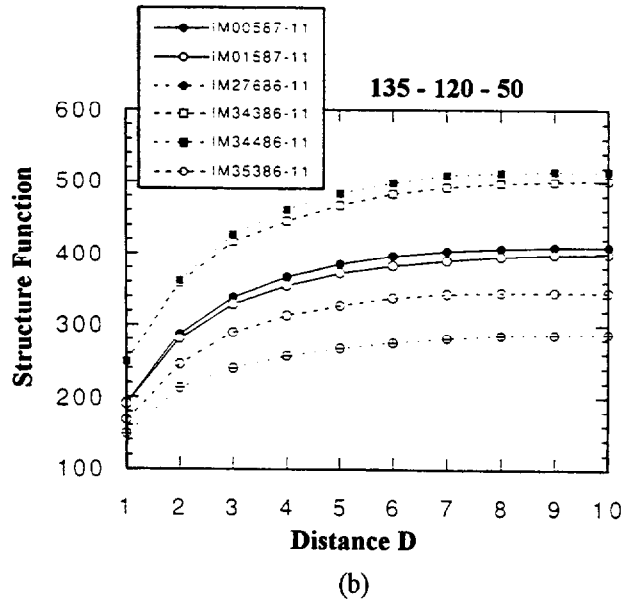
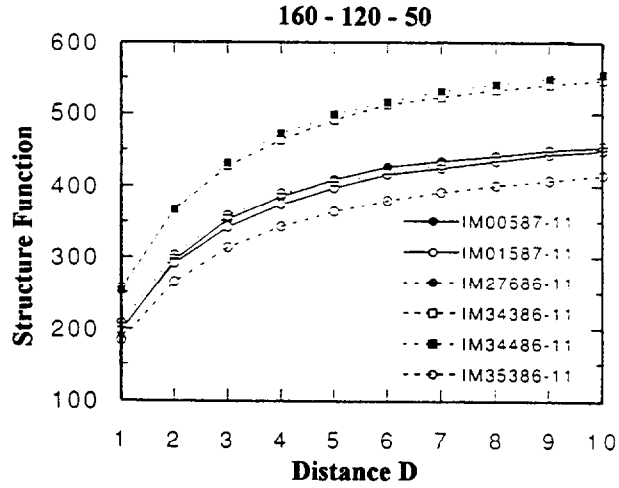
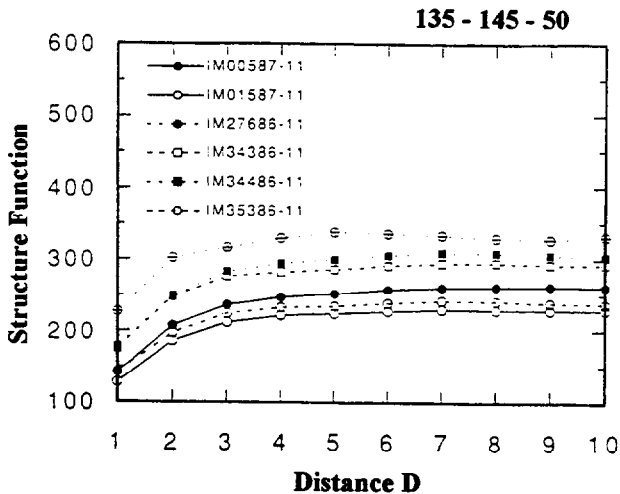


Figure 8. The structure function is plotted against the distance D for zones 1 to 3 (a, b and c respectively). Note the decrease in structure function for zone 3 compared with zones 1 and 2.



(c)

Figure 8 continued.

Using the clearest day (344) as the reference day (Table 2), and assuming the surface as invariant, from Equation (4), plots of $F^*(d)$ as a function of $F^*(d)$ for day 344 should be straight lines and slopes should be directly related to the function $T(\tau, \mu_V) F_d(\tau, \mu_S)$. Zone 1 and 2 (Figures 9a and 9b) show excellent linearity as indicated by theory, except for day 276. Linear correlation coefficients for each date are greater than 0.9992 for all days (except for 276) for zones 1 and 2 but are generally lower for zone 3 (Table 3). For day 276, starting at $d = 5$, the points deviate from a straight line - a finding more obvious for zone 2 than for zone 1. This probably results from actual surface changes since day 276 corresponds to the end of the rainy season and is about 3 months earlier than the other days. For zone 3, the linearity for any day is lower than for zones 1 and 2 possibly due to the lack of structure, a non-uniform atmosphere and/or to changes in the surface reflectance (Figure 9c) as shown by the lower correlation coefficients. At this point, we do not know exactly the relative contributions of the uncertainties.

The aerosol characteristics are taken from Shettle's (1984) background desert aerosol model. Since the geometrical conditions are known, the only remaining unknown is the aerosol optical thickness, but this can be interpreted from the slopes of the $F^*(d)$ plots (Figure 9). Comparison of the three zones and the ground measurements show variable results for zone 3 but good overall agreement for zones 1 and 2 (Figure 10). Based on these results we estimate the accuracy to be around 0.1 for the derivation of the aerosol optical thickness.

Table 3. Linear correlation coefficients (r) of the structure function for each date vs the reference date, 344. Note the low values for zone 3 and day 276 for all zones.

Day of Year	Zone 1 (r)	Zone 2 (r)	Zone 3 (r)
276	0.99910	0.99866	0.98011
343	0.99983	0.99967	0.99749
344	1.00000	1.00000	1.00000
353	0.99922	0.99968	0.99939
005	0.99974	0.99991	0.99947
015	0.99962	0.99975	0.99916

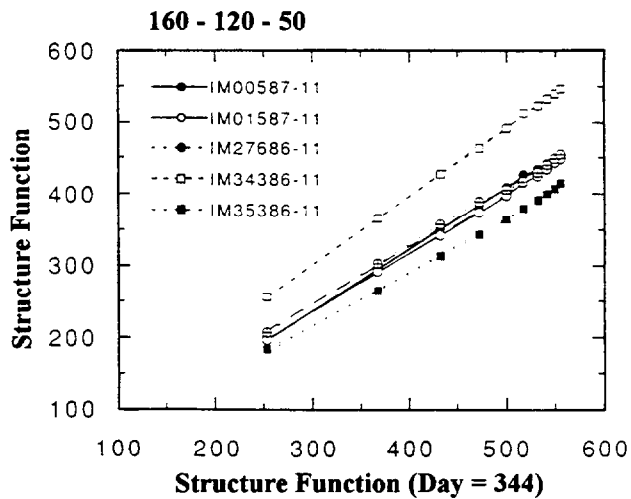
As well as the lack of structure, some of the discrepancies observed for zone 3 may result from inhomogeneities in the horizontal distribution of the aerosol optical thickness specifically within that zone. Furthermore we have assumed the same aerosol model for all turbidity conditions. D'Almeida *et al.* (1991) found that the radiative properties of the aerosol change relative to the importance of the dust events. They suggest a higher value of the asymmetry parameter resulting from a larger particle size. Considering this, the extreme point of Figure 10 would be closer to the 1:1 line but without more information on the atmosphere and ground conditions it is difficult to draw any further conclusions.

4. Large Area Application

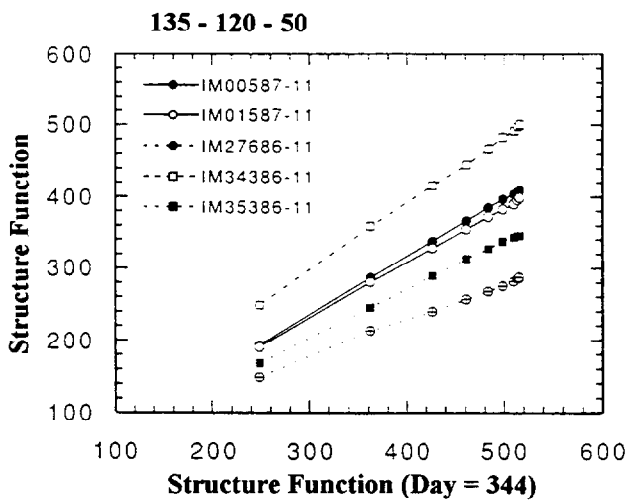
In the following section, a pilot study example of aerosol retrieval and atmospheric correction using AVHRR data for a much larger part of the Earth is provided. It covers the application of an operational atmospheric correction scheme actually tested on the zone covering the area of 60°S to 60°N and 135° West to 30° East. In contrast to the previous section, the analysis is based on GAC data.

4.1. PREPROCESSING

4.1.1 *Data set.* The Global Archive Collection (GAC) is a level 1B product from NOAA consisting of raw data for all AVHRR channels with a nominal spatial resolution 4.4 km x 5 km at nadir, degrading to 20 km x 5 km at the extreme off-nadir view ($\pm 55.0^\circ$) (see Chapters by Belward and Kidwell for more details about GAC data). This archive represents a large data volume of approximately 200 Megabytes a day for all of the Earth, but one of considerable information content. In this case study, the visible and near-infrared channels are used to derive aerosol optical thickness by correcting for broad-band, water vapour absorption for channel 2 and sensor sensitivity degradation. The preprocessing of the data is described briefly below, and the reader is referred to following chapters for more detailed discussion of preprocessing methodologies and details.

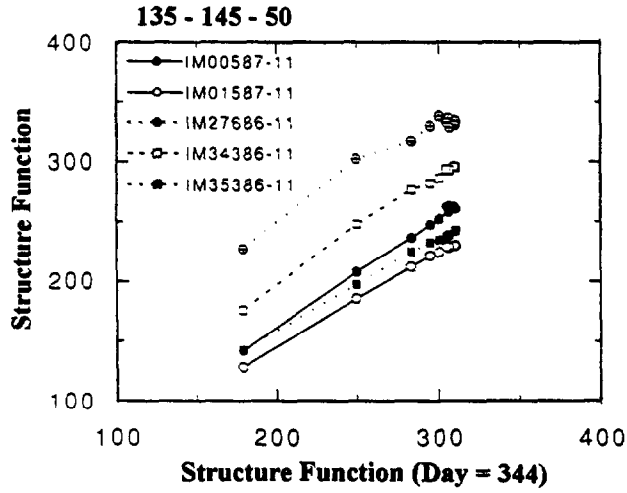


(a)



(b)

Figure 9. The structure function for all days is plotted against the reference day, 344, for zones 1, 2 and 3 (a, b and c respectively). The slopes of the lines are a function of the aerosol optical thickness.



(c)

Figure 9 continued.

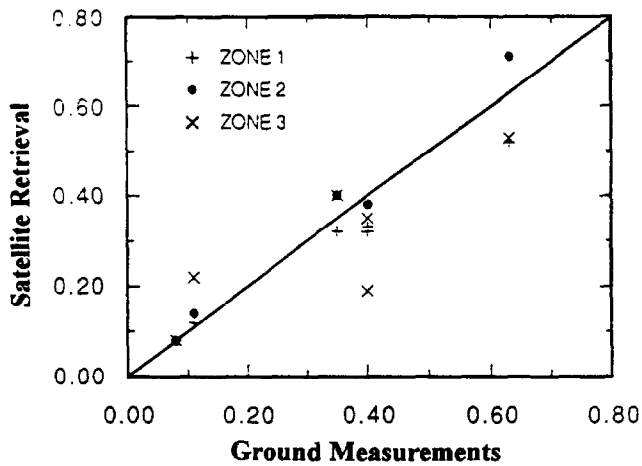


Figure 10. The satellite retrieval from the contrast reduction method is plotted against ground observations for the three zones. Zones 1 and 2 show good agreement with ground truth.

4.1.2. *Calibration.* The GAC data used for this case study were preprocessed in the following way: the reflective channels were unpacked, corrected for dark current responses and scaled to 16-bit digital numbers using pre-flight published calibration coefficients, and the thermal channels were unpacked and converted to temperature values in 16-bits (using on-board information and a non-linearity correction algorithm (Weinreb *et al.* 1990)).

4.1.3. *Cloud Screening.* The CLAVR algorithm developed by Stowe *et al.* (1991) was applied immediately after the unpacking and preflight calibration. The CLAVR algorithm used produces a mask of Ocean/Land/Cloud/DDV/elevation which is used in the next processing step. The DDV is a marker for dense dark vegetation deduced from the channel 3 reflectance which in turn is derived from channel 3, 4 and 5 brightness temperatures assuming an emissivity of 1.0 in each channel. A water vapour correction was applied by using the split-window technique (see Chapter by Vogt). The elevation of the target is used to adjust the Rayleigh correction to the effective amount of scattering by air molecules (see *Rayleigh and Ozone correction* below).

4.1.4. *Geometric Correction.* The output of the preprocessing stage is a linear lat/long grid covering the study area. An inverse navigation scheme was then used to fill this grid with the appropriate pixels extracted from the GAC Level 1B data set. This scheme uses an orbital model based on a Brouwer-Lyddane model to propagate orbital elements supplied by the US Navy ephemeris to the scene time. The propagated orbital elements are then used to resample the satellite data to fit the predefined geographic grid.

4.1.5. *Rayleigh and Ozone correction for Channel 1 and 2.* The consensus of several international working groups on AVHRR products (Faizoun 1992, Townshend 1992) was to make a first-level correction to the visible and near-infrared channel using the reference degradation correction calibration coefficient (Holben *et al.* 1990). The correction terms are the Rayleigh scattering and ozone (T_{gozone}) and oxygen (T_{goxygen}) gaseous transmission (Equation 5). The Rayleigh correction takes into account the elevation of the target and is very accurate (Vermote and Tanré, 1992). The gaseous transmission formulae are simple expressions derived from radiative transfer code runs (Tanré *et al.* 1990, Tanré *et al.* 1992).

$$\rho_{\text{cor}} = \frac{\text{Albedo}}{X_a} - \rho_{\text{Rayleigh}} \frac{P(z)}{P_0} \quad (5)$$

where :

X_a	is the product: $d T_{\text{gozone}} T_{\text{goxygen}} \cos(\text{Solar Zenith angle}) r$,
r	is the degradation coefficient (Holben <i>et al.</i> , 1991),
d	is the correction term for the variation of the Sun-Earth distance,
ρ_{Rayleigh}	is the reflectance due to molecular scattering,
Albedo	is the digital count corrected from dark current and calibrated with pre-flight calibration,
$P(z)$	is the pressure at target altitude (z) and P_0 is pressure at sea level.

4.2. AEROSOL RETRIEVAL METHODS

4.2.1. *Over water.* Once the ocean signal is corrected for Rayleigh scattering and the gaseous transmission effect, the radiance observed in channel 1 is due mainly to aerosol scattering. Using a radiative model simulating the reflectance above a rough ocean (Deuzé *et al.* 1989), we derived, for several optical thickness values (from 0.0 to 1.0 at $0.55 \mu\text{m}$), the reflectance that would be observed by the sensor in case of a maritime model for a wind speed of 10 ms^{-1} . In the glint pattern, simulations are highly dependent on the wind speed so we only inverted data outside a cone of 30 degrees around the specular reflection. We also limited the retrieval to cloud-free pixels only.

In channel 2, the effect of the water vapour should also be corrected for. As its effect varies strongly with time and space, it is important to obtain the water vapour content at the same time and in the same conditions as the radiance. Several published studies have used T_4 - T_5 for the retrieval of the amount of water vapour in the atmosphere (*e.g.* Dalu 1986).

Using more than one year of SSMI and AVHRR data over the Pacific Ocean, a relation between the water vapour content and T_4 - T_5 has been established. We assume that water vapour content is linearly proportional with T_4 - T_5 , *i.e.*: $U_{\text{H}_2\text{O}} = A(\theta) \cdot (T_4 - T_5)$. A plot of SSMI water vapour content versus nadir measurements of T_4 - T_5 is given in Figure 11. The coefficient A can then be deduced $A(0^\circ) = 1.98 \pm 0.5 \text{ g/cm}^2/\text{K}$. For a viewing angle $\theta = 60^\circ$, this coefficient becomes (see Figure 12) $A(60^\circ) = 1.53 \pm 0.5 \text{ g/cm}^2/\text{K}$.

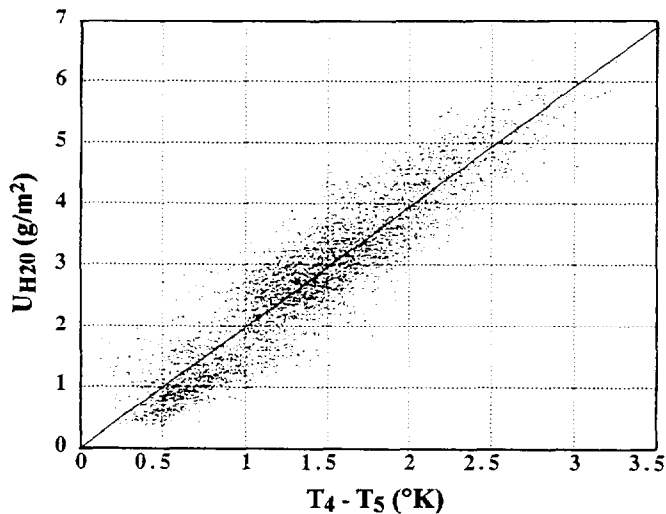


Figure 11. Plot of the water vapour amount (SSMI) versus T_4 - T_5 (AVHRR) measured over the Pacific Ocean for a viewing angle of 0° .

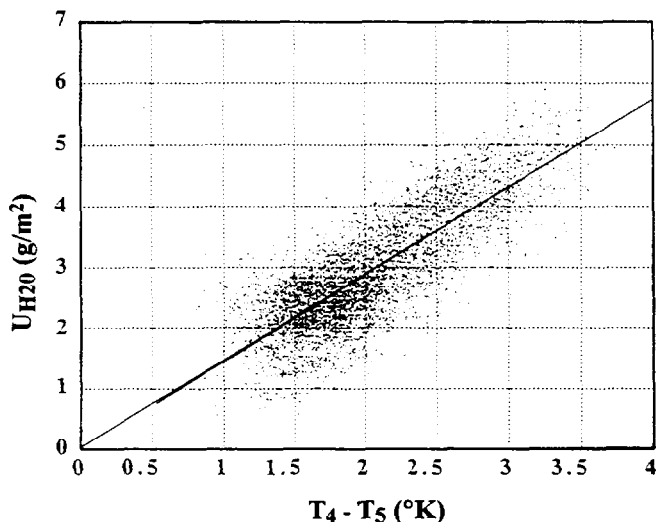


Figure 12. Plot of the water vapour amount (SSM/I) versus $T_4 - T_5$ (AVHRR) measured over the Pacific Ocean for a viewing angle of 60° .

The angular dependency for some values of the $\cos(\theta)$ is shown in Figure 13. The retrieved results are then compared with theoretical computations. Defining 36 different atmospheres with a water vapour content ranging from 0 to 6.5 g/cm^2 , we computed (with Lowtran 7) the coefficient A for different angles. These computations confirm the angular dependency of the coefficient A (Figure 13) which does not seem to follow a $\cos(\theta)$ law. Once the water vapour content is estimated, the absorption due to it in channel 2 is computed from the radiative transfer model.

4.2.2. Over Land, the Dark Target concept. As mentioned in section 2, Dense Dark Vegetation (DDV) targets exhibit very low reflectance in channel 1 of the AVHRR. At this wavelength, $0.65 \mu\text{m}$, DDV can be used as a reference dark target (0.01-0.02 reflectance units) to derive the path radiance, and studies of the accuracy of the method shows that the path radiance can be used for the purpose of atmospheric correction with an accuracy of ± 0.01 . If the aerosol model is known the optical depth can be retrieved with an error of 0.10.

Detection of DDV using the channel 3 brightness temperature as an alternative to channel 1 reflectance has been assessed by Holben *et al.* (1992) where a new method using Channel 3 temperature has been introduced. In this "thermal" channel the DDV

pixels are selected because they are cooler, less reflective and more absorbent of water than bare soil or less vegetated pixels.

In this case study we tried to use the *albedo* of channel 3 instead of brightness temperature, as the latter is not suitable for global application. One expression of this albedo can be found in Stowe *et al.* (1991). It is derived from the assumption that emissivity in Channel 4 and 5 is equal to 1, and in this case, water vapour absorption can be corrected by the split-window technique. This is applicable for sea surfaces, but our goal was to give a threshold for DDV detection rather than to try to use the Channel 3 albedo quantitatively. This threshold has been arbitrarily set at 3%. Figure 14 gives a global overview of the aerosol retrieval both on sea and land. The retrieval is limited by the presence of clouds over land and ocean, and over land by the presence of DDV.

4.3. RESULTS

Figure 15 shows a comparison between optical thicknesses derived from AVHRR with sunphotometer measurements taken at Cape Grin (Australia). Agreement between the two is generally good in both channels which validates the retrieval scheme and water vapour correction. However, some discrepancy can occur due to the temporal or spatial variability of the aerosol layer.

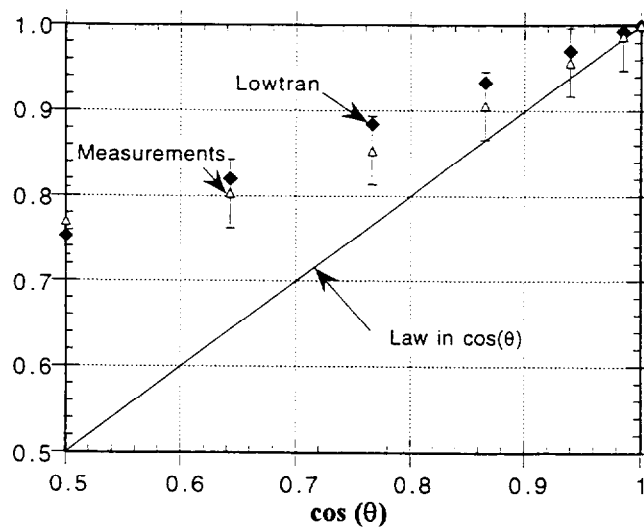


Figure 13. Angular dependency of the coefficient A (normalised to 1) determined both by the measurements and by the computations. Also reported, the law in $\cos(\theta)$.

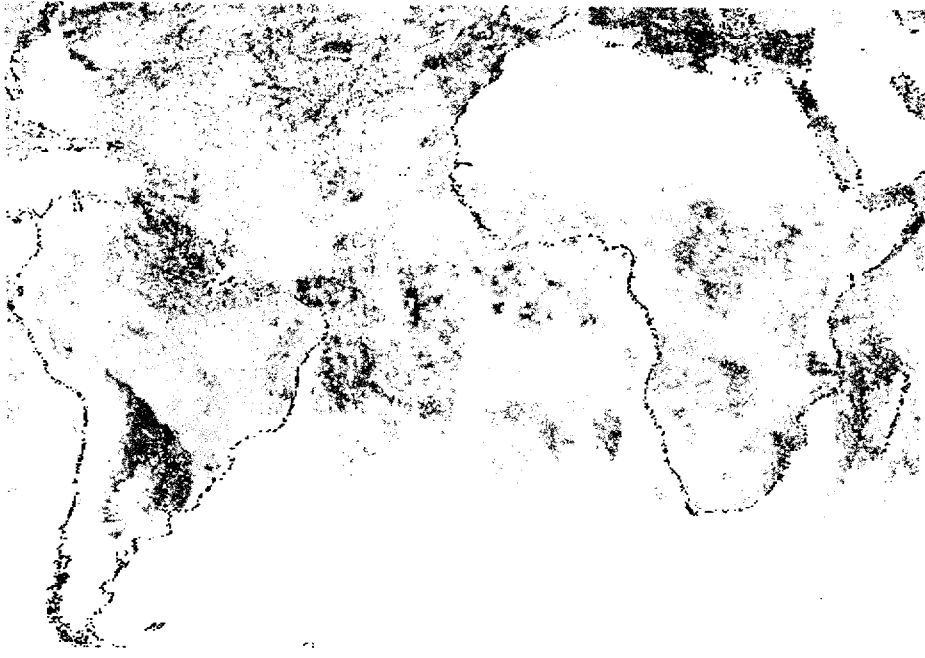


Figure 14. 550 nm aerosol depth maximum values retrieved during the 09/03/93 - 09/09/93 period using AVHRR-NOAA-11 data. Values range from 0.1 to 2.0 (over Brazil) due to biomass burning.

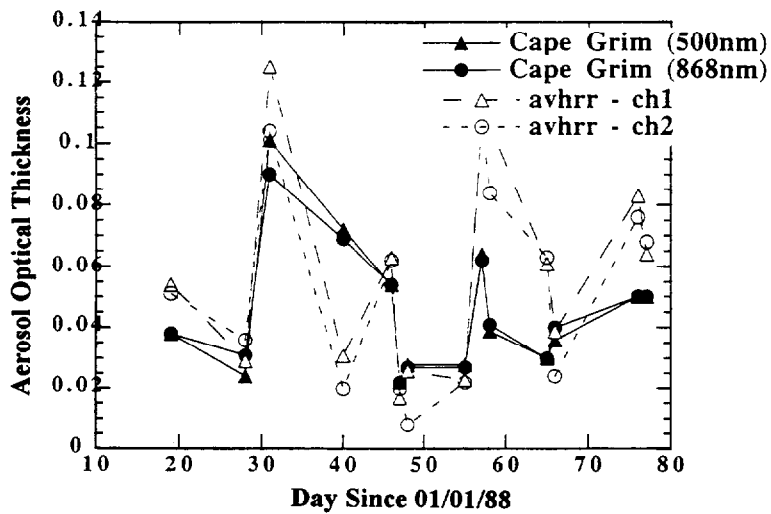


Figure 15. Comparison of optical thicknesses inverted from AVHRR channel 1 and 2 with sunphotometer measurements made at Cape Grim (Australia).

Figure 16 shows a comparison between optical thickness derived from DDV observation in channel 1 with sunphotometer measurements taken in Brazil (1992). The agreement between the two sets is very good considering the uncertainty on the reflectance of DDV in channel 1 (± 0.01) which translates directly to an uncertainty of 0.1 in the derived aerosol optical thickness.

4.4 CONCLUSIONS

We have presented a method for atmospheric correction and aerosol retrieval using the visible and near-infrared channels of AVHRR. The method has been applied over a very large area and a first comparison with sunphotometer measurements demonstrates the validity of the approach. Similar algorithms which will be used to correct MODIS data will be tuned using sunphotometer network results, ground measurement campaigns and validated with the current efforts to understand the dynamics of aerosol transport using historical AVHRR data sets.

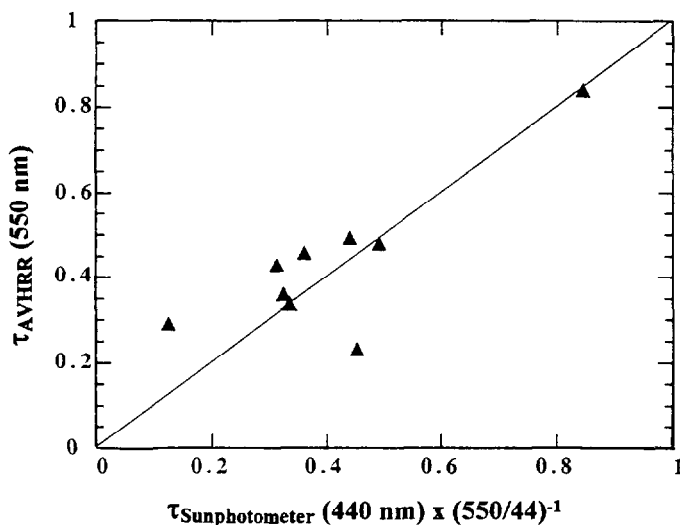


Figure 16. Comparison of optical thicknesses inverted from channel 1 of the AVHRR over Dense Dark Vegetation with sunphotometer measurements made in Brazil (1992).

5. Stratospheric aerosol perturbations (the Mount Pinatubo eruption)

The second example of the application of the aerosol retrieval and atmospheric correction methods described in this chapter, concerns the operational correction of NDVI for stratospheric aerosol effect, necessitated by the eruption of Mount Pinatubo in the Philippines on 6 June, 1991. Stratospheric aerosols produced by the eruption had a noticeable effect on NOAA-AVHRR data values. Following the eruption, a longitudinally homogeneous dust layer was observed between 20°N and 20°S. The largest optical thickness observed for the dust layer was 0.4-0.6 at 0.5 μm . Due to this layer, the monthly composite Normalized Difference Vegetation Index (NDVI) (generally bounded between -0.1 and 0.6) has shown a systematic decrease of up to 0.15 units, two months after the eruption. Such an atmospheric effect has never previously been observed, and its persistence and spatial extent has seriously compromised the validity of the compositing technique. It stresses that long term monitoring of vegetation using the NDVI necessitates correction of the effect of stratospheric aerosols.

The correction scheme we describe here consists of the examination of a latitudinal profile of optical thickness in channels 1 and 2 over the Pacific Ocean, and use of a radiative transfer code assuming lambertian boundary conditions to correct each pixel in the two channels prior to computing the NDVI.

5.1. DETERMINATION OF THE LATITUDINAL PROFILE OF STRATOSPHERIC OPTICAL DEPTH.

A few months after Mount Pinatubo injected aerosols into the upper atmosphere, stratospheric winds produced a longitudinally homogeneous aerosol layer (Stowe *et al.* 1992). This allowed us to derive a stratospheric aerosol optical thickness latitudinal profile by using data from the Pacific Ocean only. This area is known to have a low loading in tropospheric aerosols.

The part of the signal corresponding to stratospheric aerosols can be extracted by subtracting from the total signal, that part produced by the ocean and other atmospheric effects. The latter is determined theoretically by considering a clear ocean with a nominal tropospheric aerosol load. A stratospheric aerosol model (King *et al.* 1984) is then used to invert the measured signal and deduce the optical depth for different solar and viewing geometry. Figures 17 and 18 give the measured normalised radiance contributed by stratospheric aerosols for channels 1 and 2 (solid line) and theoretical contributions of stratospheric aerosols in these channels computed by King's model for an optical depth of 0.4 (dotted lines). The theoretical plots intercept the measured ones in the same area (latitudinal range) for both channels and for the two different viewing angles considered in these figures. These important features show the spectral and geometric consistency of the model.

With this technique applied to cloud-free weekly composited images of channels 1 and 2 (Figure 19), the values obtained for different zenith angles are averaged to produce the latitudinal profile (Figure 20).

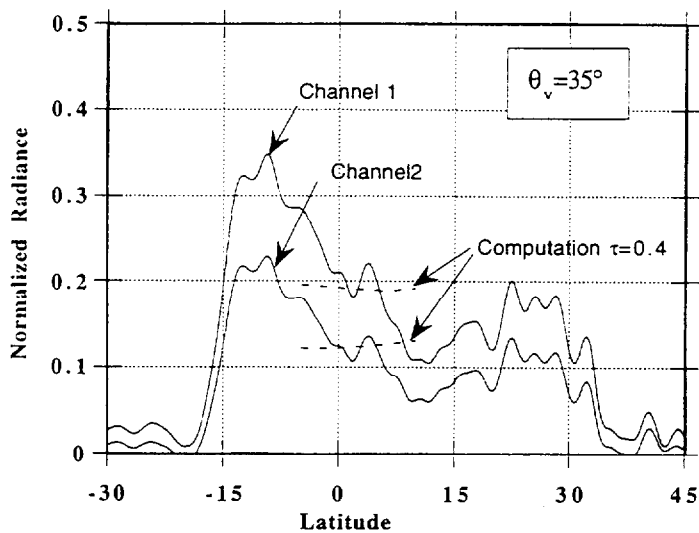


Figure 17. Comparison of the Pinatubo radiances observed at 35° view angle with radiative transfer computation.

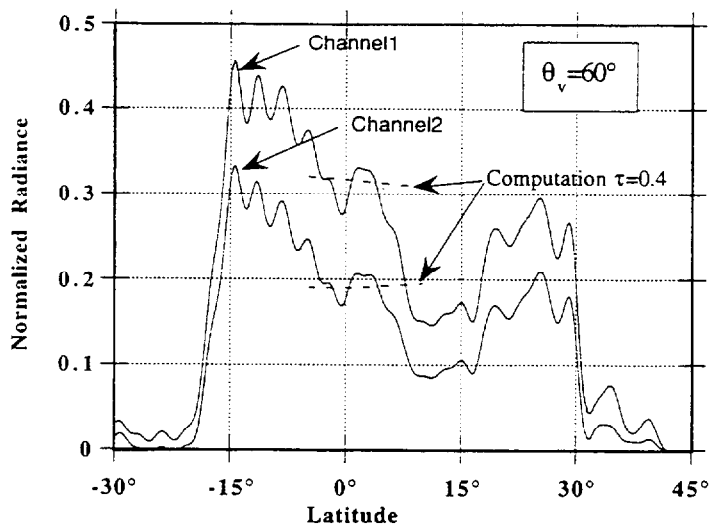
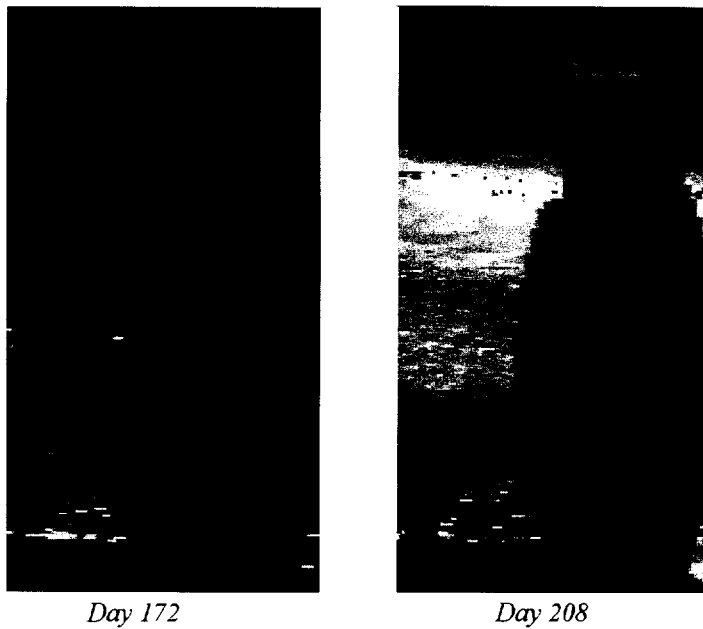


Figure 18. Comparison of the Pinatubo radiances observed at 60° view angle with radiative transfer computation.



OPTICAL THICKNESS

Figure 19. "Geometric" composite of the optical thickness observed in channel 1 of the AVHRR before (a) and after the stratospheric aerosol layer formation (b). The top of the image corresponds to a latitude of -60°S , the bottom to $+60^{\circ}\text{N}$.

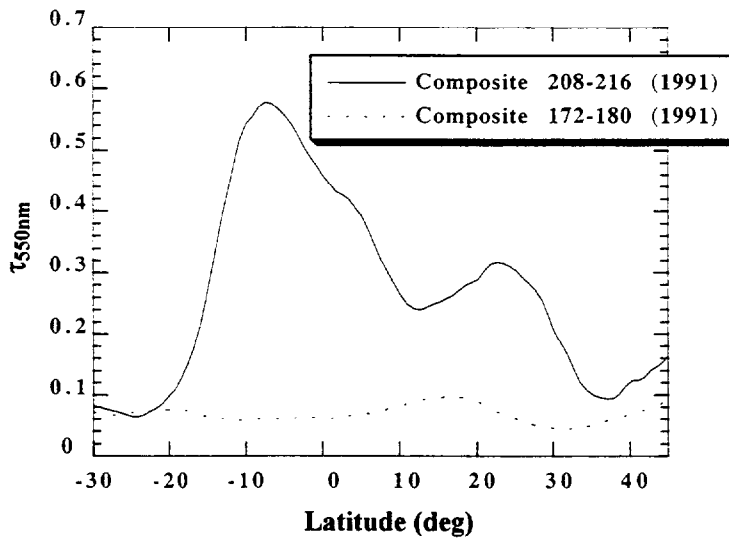


Figure 20. Stratospheric Profiles deduced from Figure 3.

5.2. CORRECTION EQUATION FOR NDVI 30-DAY COMPOSITE

The NDVI is computed from AVHRR visible (0.63 μm) and near infrared (0.87 μm) pre-flight calibrated digital counts, DC_1 and DC_2 as follows:

$$\text{NDVI} = \frac{DC_2 - DC_1}{DC_2 + DC_1} \quad (6)$$

Considering only the effect of stratospheric perturbations, the measured digital counts for channels 1 and 2 can be written as

$$DC^{\text{perturbed}} = DC^{\text{stratosphere}}(\phi) + T(\mu_s)T(\mu_v)DC^{\text{corrected}} \quad (7)$$

Where μ_s , μ_v and ϕ are the cosine of the solar zenith angle, the cosine of the view angle and the azimuth difference between the Sun and the sensor respectively and $DC^{\text{stratosphere}}$ is the measured value of the stratospheric aerosol path radiance (see section 3.1).

$T(\mu)$ is the transmission (upward for μ_v , downward for μ_s) of the aerosol layer computed using King's model (King *et al.* 1984) and optical thickness deduced in section 3.1. The corrected values of channels 1 and 2 are deduced from Equation 7.

5.3. RESULTS AND DISCUSSION

The method described above has been applied over an area in East Africa (-10°S, 10°N). All 10-day composites of the NDVI have been computed for 1989/90/91 before and after the eruption. Figure 21 shows the histograms of the results obtained before eruption. The values computed for 1991 are comparable with the historical data of 1989 and 1990. In Figure 22 (after eruption) the histogram corresponding to the uncorrected values shows a decrease in the NDVI. Applying the correction algorithm reinstates the values back to their expected range. The same kind of test has been performed for 1992, and its results are given in Figure 23.

5.4. CONCLUSIONS

This method has been developed as a quick and effective procedure that can be applied operationally to the generation of NDVI from AVHRR data, corrected for stratospheric aerosol effects. The first results are very encouraging and an extended validation is ongoing as well as the preparation of a direct method directly applicable to NDVI values.

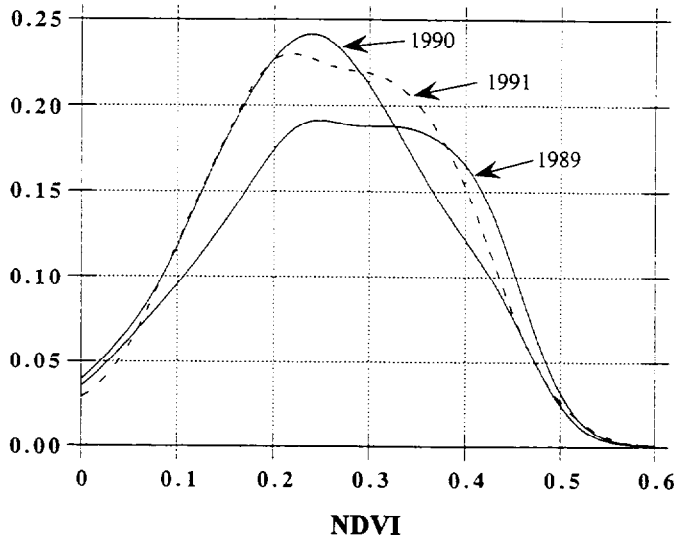


Figure 21. Histogram of NDVI over Africa (-10°S , $+10^{\circ}\text{N}$) for three years prior to the Pinatubo eruption.

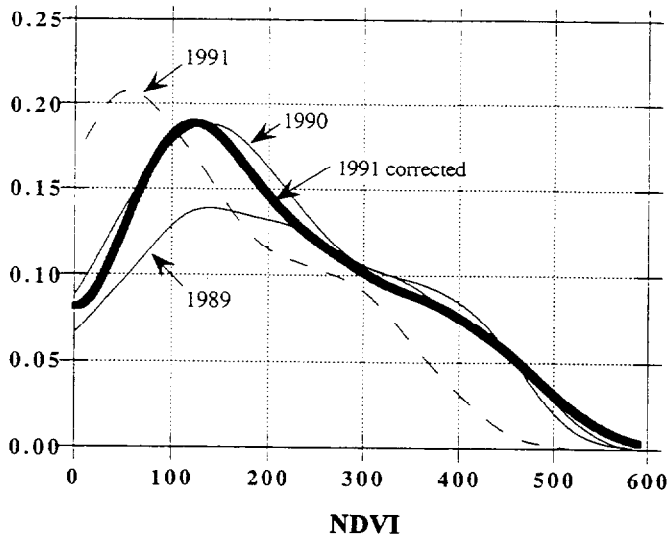


Figure 22. Histogram of NDVI over Africa (-10°S , $+10^{\circ}\text{N}$) for three years prior to the Pinatubo eruption. Also included is the post-eruption period (August), and corrected values of NDVI for 1991.

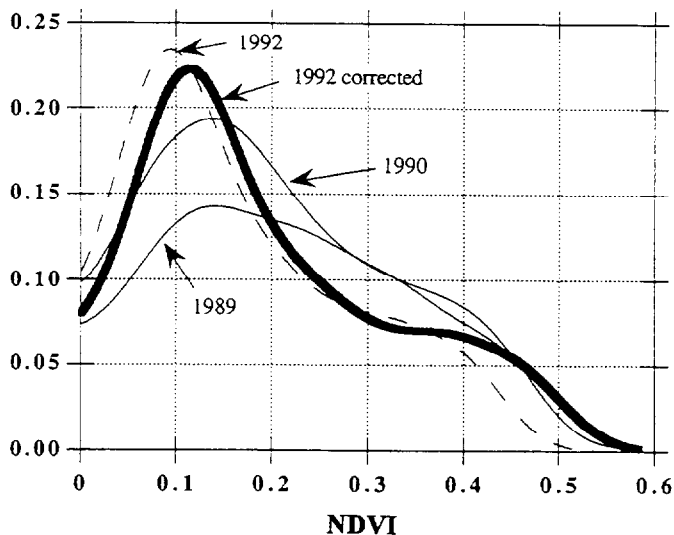


Figure 23. Histogram of NDVI over Africa (-10°S , $+10^{\circ}\text{N}$) for two years prior to the Pinatubo eruption. Also included is the post-eruption period (August), and corrected values of NDVI for 1992.

6. Summary

Analysis of time-series data for detection and monitoring of changes in earth or atmospheric parameters requires detailed correction for atmospheric effects. We have presented here the current state of a quasi-operational atmospheric correction procedure for AVHRR data. Included in this procedure is an aerosol retrieval scheme applicable for oceans and forested land surfaces. Aerosol retrievals are also possible for land surfaces not covered by forests, but an operational algorithm is still to be developed.

Application of the dark target approach to a subset of the global landmass archive showed good results when compared with available ground measurements. For vegetation monitoring, a further correction for low frequency variations of stratospheric aerosol (for example due to the eruption of Mount Pinatubo) is also necessary, and a method using part of the AVHRR global archive has been developed and presented. This shows good agreement to pre-Pinatubo years.

Thus, the corrective methods reviewed and presented here have shown global applicability for long historical time-series data obtained from the NOAA-AVHRR archive, and the application of these techniques are anticipated to provide more realistic and more reliable measurements of earth and atmospheric parameters from long time-series of data. The demonstration of their usefulness to global-scale data sets also encourages us to promote their development and application to forthcoming EOS global-scale data sets.

References

- Arking, A. and Childs, J., 1985, Retrieval of cloud cover parameters from multispectral satellite images. *Journal of Climate and Applied Meteorology*, **24**, 322-333.
- D'Almeida, G.A., Koepke, P. and Shettle, E.P., 1991. Atmospheric Aerosols Global Climatology and Radiative Characteristics (Hampton: A Deepak Publishers).
- Dalu, G., 1986, Satellite remote sensing of atmospheric water vapor. *International Journal of Remote Sensing*, **7**, 9, 1089-1097.
- Deering, D. W. and Eck, T. F., 1991, Directional Radiance Distributions above and within a forest canopy Ch285-8/90/0000-0879/\$01.00, NASA/GSFC,
- Deuzé, J. L., Herman, M. and Santer, R., 1989, Fourier series expansion of the transfer equation in the atmosphere-ocean system. *Journal of Quantitative Spectroscopy and Radiative Transfer*, **41**, 6, 483-494.
- Faizoun, A. C., 1992, Final Report of the OSS Working Group on NOAA-AVHRR Standard Preprocessing Definition 1, LERTS,
- Holben, B., N, Eck, T. and Fraser, R., S, 1991, Temporal and spatial variability of aerosol optical depth in the Sahel region in relation to vegetation remote sensing. *International Journal of Remote Sensing*, **12**, 6, 1147-1163.
- Holben, B. N., Kaufman, Y. J., Setzer, A., Tanré, D. and Ward, D. E., 1990, Optical properties of aerosols from biomass burning in the tropics, BASE-A. *Chapman conference on Biomass Burning*,
- Holben, B. N., 1986, Characteristics of maximum-value composite images for temporal AVHRR data. *International Journal of Remote Sensing*, **7**, 11, 1435-1445.
- Holben, B. N. and Fraser, R. S., 1984, Red and near infrared response to off-nadir viewing. *International Journal of Remote Sensing*, **5**, 145-160.
- Holben, B. N., Vermote, E., Kaufman, Y. J., Tanré, D. and Kalb, V., 1992, Aerosol retrieval over land from AVHRR data-application for atmospheric correction. *IEEE Transaction on Geoscience and Remote Sensing*, **30**, 2, 212-222.
- Kaufman, Y. J., 1991, Measurements of the Aerosol Optical Thickness and Path Radiance. *Journal of Geophysical Research*, **98**, D2, 2677-2692.
- Kaufman, Y. J. and Sendra, C., 1988, Algorithm for automatic atmospheric corrections to visible and near-IR satellite imagery. *International Journal of Remote Sensing*, **9**, 8, 1357-1381.
- Kaufman, Y. J., Setzer, A., Ward, D., Tanré, D., Holben, B. N., Menzel, P., Pereira, M. C. and Rasmussen, R, 1992, Biomass Burning Airborne and Space Borne Experiment in the Amazonas (BASE-A). *Journal of Geophysical Research*, **97**, D13, 14581-14599.
- Kerber, G. B., and Schutt, J. B., 1986, Utility of AVHRR Channels 3 and 4 in land cover mapping. *Photogrammetry Engineering and Remote Sensing*, **52**, 1877-1883.
- Kimes, D. S., Newcomb, W. W., Nelson, R. F. and Schutt, J. B., 1986, Directional Reflectance Distributions of a Hardwood and Pine Forest Canopy. *IEEE Transactions on Geoscience and Remote Sensing*, **GE-24**, 2, 281-293.
- King, M., Harshvardhan D. and Arking, A., 1984, A model of the radiative properties of the El Chichon Stratospheric Aerosol layer. *Journal of Climate and Applied*

- Meteorology*, **23**, 7, 1121-1137.
- Kleman, J., 1987, Directional Reflectance Factor Distributions for Two Forest Canopies. *Remote Sensing of Environment*, **23**, 83-96.
- Kriebel, K., T., 1977, Reflection properties of vegetated surfaces: Tables of measured spectral biconical reflectance factors. DFVLR, Internal Document.
- Lee, T. Y. and Kaufman, Y. J., 1986, Non-Lambertian effects on remote sensing of surface reflectance and vegetation index. *IEEE Transactions on Geoscience and Remote Sensing*, **GE-24**, 699-708.
- Malingreau, J. P. and Tucker, C. J., 1988, Large-scale deforestation in the southern Amazon Basin of Brazil. *Ambio*, **17**, 49-55.
- Shettle, E., P., 1984, Optical and radiative properties of a desert aerosol model. *Symposium of Radiation in the atmosphere*, 1 Deepak Publishing, pp. 74-77.
- Shettle, E. P. and Fenn, R. W., 1979, Models for the aerosol of the lower atmosphere and the effect of humidity variations on their optical properties Opt. Phys. Div., Air Force Geoph. Lab., U.S.A.
- Stowe, L. L., Carey, R. M. and Pellegrino, P. P., 1992, Monitoring the Mt. Pinatubo aerosol layer with NOAA/11 AVHRR data. *Geophysical Research Letter*, **19**, 2, 159-162.
- Stowe, L. L., McClain, E. P., Carey, R., Pellegrino, P., Gutman, G. G., Davis, P., Long, C. and Hart, S., 1991, Global Distribution of Cloud Cover derived from NOAA/AVHRR operational Satellite Data. *Advances in Space Research / COSPAR*, 11 COSPAR), pp. 51-54.
- Tanré, D., Deroo, C., Duhaut, P., Herman, M., Morcette, J. J., Perbos, J. and Deschamps, P. Y., 1990, Description of a computer code to simulate the satellite signal in the solar spectrum "5S code". *International Journal of Remote Sensing*, **11**, 659-668.
- Tanré, D., Deschamps, P. Y., Devaux, C. and Herman, M., 1988, Estimation of Saharan aerosol optical thickness from blurring effects in Thematic Mapper data. *Journal of Geophysical Research*, **92**, 15955-15964.
- Tanré, D., Holben, B. N. and Kaufman, Y. J., 1992, Atmospheric Correction algorithm for NOAA-AVHRR Products: Theory and Application. *IEEE Transaction on Geoscience and Remote Sensing*, **30**, 2, 231-248.
- Townshend, J. R. G., 1992, Improved Global Data for Land Applications: A proposal for a New High Resolution Data Set 20, IGBP,
- Tucker, C., J., Holben, B., N and Goff, T., E., 1984, Intensive forest clearing in Rondonia, Brazil, as detected by satellite remote sensing. *Remote Sensing of Environment*, **15**, 255.
- Vermote, E. F. and Tanré, D., 1992, Analytical Expressions for Radiative Properties of Planar Rayleigh Scattering Media Including Polarisation Contribution. *Preprint for Journal of Quantitative Spectroscopy and Radiative Transfer*, **47**, 4, 305-314.
- Weinreb, M. P., Hamilton, G., Brown, S. and Koczor, R. J., 1990, Nonlinearity Corrections in Calibration of Advanced Very High Resolution Radiometer Infrared Channels. *Journal of Geophysical Research*, **95**, C5, 7381-7388.
- Whitby, K., T., 1978, The physical characteristics of sulfur aerosols. *Atmospheric Environment*, **12**, 135-159.